

Rabi Oscillations in a Large Josephson-Junction Qubit

John M. Martinis, S. Nam, and J. Aumentado*

National Institute of Standards and Technology, 325 Broadway, Boulder, Colorado 80305-3328

C. Urbina†

Service de Physique de l'Etat Condensé, Commissariat à l'Energie Atomique, Saclay, F-91191 Gif-sur-Yvette Cedex, France

(Received 16 March 2002; published 21 August 2002)

We have designed and operated a circuit based on a large-area current-biased Josephson junction whose two lowest energy quantum levels are used to implement a solid-state qubit. The circuit allows measurement of the qubit states with a fidelity of 85% while providing sufficient decoupling from external sources of relaxation and decoherence to allow coherent manipulation of the qubit state, as demonstrated by the observation of Rabi oscillations. This qubit circuit is the basis of a scalable quantum computer.

DOI: 10.1103/PhysRevLett.89.117901

PACS numbers: 03.67.Lx, 03.65.Yz, 74.50.+r, 85.25.Cp

The question of the applicability of the laws of quantum mechanics to macroscopic degrees of freedom triggered some 20 years ago [1] the development of superconducting junction circuits displaying quantum behavior at the level of their macroscopic electrical variables. Energy level quantization [2], macroscopic quantum tunneling [3], and quantum superposition of states [4–6] have indeed been observed in these “atomlike” circuits. More recently, the idea that quantum mechanics could be used to manipulate information efficiently [7] has boosted interest from a different perspective for such solid-state devices: the two lowest energy states of these circuits could be used as a quantum bit (qubit) and scaled to a full quantum computer through integrated-circuit technology. However, as solid-state qubits are by necessity coupled to many electromagnetic degrees of freedom through bias and measurement wires, long coherence times requires careful circuit design [8].

Circuits presently being explored combine in variable ratios the Josephson effect and single Cooper-pair charging effects. When the Josephson energy is dominant, these “flux circuits” are sensitive to external flux and its noise [6,9,10]. Conversely, when the Coulomb energy is dominant, the “charge circuits” can decohere from charge noise generated by the random motion of offset charges [11,12]. For the intermediate-energy regime, a circuit designed to be insensitive to both the charge and flux bias has recently achieved [13] long coherence times (500 ns), demonstrating the potential of superconducting circuits.

In this Letter, we present a new qubit designed around a 10 μm scale Josephson junction in which the charging energy is very small, thus providing immunity to charge noise. Although still sensitive to flux, the circuit retains the quality of being tunable, and calculations indicate that decoherence from flux noise is small. Built into the circuit is a single-shot state measurement that has good fidelity. However, the most significant advantage is that scaling to more complex circuits will be favorable be-

cause fabrication and operation of complex superconducting integrated circuits with *large* junctions are well established. Moreover, the large junction capacitance enables qubits to be capacitively coupled over relatively long distances, allowing greater and more easily engineered interconnectivity.

The quantum properties of the current-biased Josephson junction [Figs. 1(a) and 1(b)] are well established [3]. With zero dc voltage across the junction, the Josephson inductance and the junction capacitance form an anharmonic “LC” resonator in which the two lowest quantized energy levels are the states of the qubit. Because the junction bias current I is typically driven close to the critical current I_0 , the anharmonic potential can be well approximated by a cubic potential

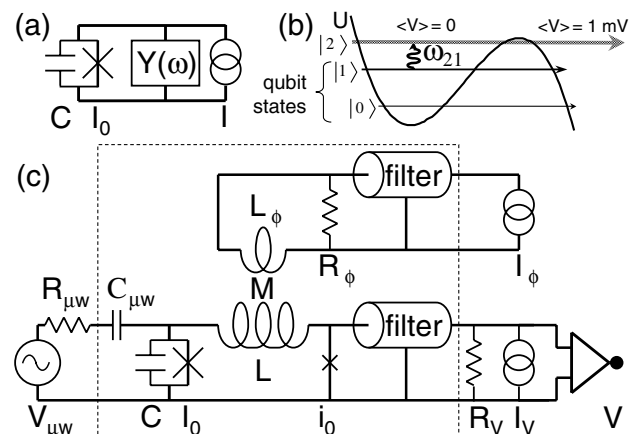


FIG. 1. (a) Model for a current-biased Josephson junction. (b) Cubic potential U showing qubit states and measurement scheme. (c) Circuit diagram for a qubit with high-impedance current bias. Dashed box indicates components fabricated on a superconducting integrated circuit. Microwaves are injected via $C_{\mu w}$. Component values are $I_0 \approx 21 \mu\text{A}$, $C \approx 6 \text{pF}$, $i_0 \approx 10.5 \mu\text{A}$, $C_{\mu w} \approx 2 \text{fF}$, $R_{\mu w} \approx 50 \Omega$, $L \approx 3.3 \text{nH}$, $M \approx L/160$, $L_\phi \approx 0.4 \text{nH}$, $R_\phi \approx 2 \Omega$, and $R_V \approx 50 \Omega$.

parametrized by the potential barrier height $\Delta U(I) = (2\sqrt{2}I_0\Phi_0/3\pi)[1 - I/I_0]^{3/2}$ and a (classical) plasma oscillation frequency at the bottom of the well $\omega_p(I) = 2^{1/4}(2\pi I_0/\Phi_0 C)^{1/2}[1 - I/I_0]^{1/4}$, where $\Phi_0 = h/2e$. Note that, as $I \rightarrow I_0$, ΔU decreases rapidly to zero while ω_p decreases much more slowly. The bound quantum states $|n\rangle$ with energy E_n can be observed spectroscopically by resonantly inducing transitions with microwaves at frequencies $\omega_{mn} = E_{mn}/\hbar = (E_m - E_n)/\hbar$. For typical operation, the number of states in the well is approximately $\Delta U/\hbar\omega_p \sim 3$, the transition frequency between qubit states is $\omega_{10} \approx 0.9\omega_p$, and the separation of the two lowest resonant frequencies is $\omega_{10} - \omega_{21} \approx 0.1\omega_{10}$. For the $|1\rangle$ state, the decay rate $\gamma_1 \approx \text{Re}Y(\omega_{10})/C \equiv \omega_{10}/Q$ is approximately the classical rate of energy decay [14], where $\text{Re}Y$ is the real (dissipative) part of the admittance of the current bias and Q is the oscillator quality factor. The rates Γ_n of tunneling out of states $|n\rangle$ are given by $\Gamma_0 \approx 52(\omega_p/2\pi)\sqrt{\Delta U/\hbar\omega_p} \exp[-7.2\Delta U/\hbar\omega_p]$ and $\Gamma_{n+1}/\Gamma_n \sim 1000$.

The qubit state can be fully manipulated with dc and microwave pulses of bias current

$$I(t) = I_{\text{dc}} + \delta I_{\text{dc}}(t) + I_{\mu\text{wc}}(t) \cos\omega_{10}t + I_{\mu\text{ws}}(t) \sin\omega_{10}t.$$

Under the condition that δI_{dc} , $I_{\mu\text{wc}}$, and $I_{\mu\text{ws}}$ are varied in time slowly compared to $2\pi/(\omega_{10} - \omega_{21}) \sim 1$ ns, the dynamics of the system is restricted to the Hilbert space spanned by the lowest two states and has a Hamiltonian in the ω_{10} rotating frame

$$H = \hat{\sigma}_x I_{\mu\text{wc}}(t) \sqrt{\hbar/2\omega_{10}C}/2 + \hat{\sigma}_y I_{\mu\text{ws}}(t) \sqrt{\hbar/2\omega_{10}C}/2 + \hat{\sigma}_z \delta I_{\text{dc}}(t) (\partial E_{10}/\partial I_{\text{dc}})/2,$$

where $\hat{\sigma}_{x,y,z}$ are Pauli operators.

The measurement of the qubit state utilizes the escape from the cubic potential via tunneling. To measure the occupation probability p_1 of state $|1\rangle$, we pulse microwaves at frequency ω_{21} , driving a $1 \rightarrow 2$ transition. The large tunneling rate Γ_2 then causes state $|2\rangle$ to rapidly tunnel. After tunneling, the junction behaves as an open circuit, and a dc voltage of the order of the superconducting gap (~ 1 mV) appears across the junction. This voltage is readily measured with a room-temperature amplifier. Thus the occupation probability p_1 is equal to the probability p_v of observing a voltage across the junction after the measurement pulse.

The manipulation of the qubit over many logic pulses requires a large Q . In turn, this imposes both a small energy relaxation rate γ_1 and a small dephasing rate from low frequency noise in the current bias. Both these conditions are met by using a current bias with high impedance from dc to frequencies $\geq \omega_p/2\pi \sim 10$ GHz. We can obtain $Q \geq 10^5$ for junctions of area $\sim 100 \mu\text{m}^2$ ($C \sim 10$ pF) with $1/\text{Re}Y \geq 160$ k Ω . This cannot be achieved with a conventional current bias since typical wire impedances at microwave frequencies are low ($\sim 100\Omega$).

Figure 1(c) shows a circuit that realizes this high-impedance current bias using broadband transformers. Because of the large loop inductance $L \gg L_{J0} = \Phi_0/2\pi I_0$, the circuit creates a current divider from the external biases to the bias current of the qubit junction $I \approx (M/L)I_\phi + (L_{Jf}/L)I_V$. These current dividers produce transformations in $1/\text{Re}Y$ of $(L/M)^2$ and $(L/L_{Jf})^2$. Here the ‘‘filter’’ junction (labeled i_0) behaves as an inductor [15] with value $L_{Jf} = \Phi_0/2\pi i_0$ because its current $I_V - (M/L)I_\phi$ is made small by adjusting the biases such that $I_V \approx (M/L)I_\phi$. For the particular design of Fig. 1(c), a full calculation shows that the dominant dissipation source gives $1/\text{Re}Y \approx (L/L_{Jf})^2 R_V \approx 560$ k Ω .

The qubit circuit of Fig. 1(c) is fabricated with a standard niobium trilayer process using optical lithography. The inductor L is a six-turn spiral to minimize radiation damping and to keep its self-resonant frequency ~ 15 GHz much larger than $\omega_p/2\pi$. The chip is mounted inside a doubly shielded Cu and Al box anchored to the mixing chamber of a dilution refrigerator whose base temperature is 25 mK. The microwave line is attenuated and bias lines heavily filtered with Cu powder and RC filters [16]. Low-noise bias currents are generated with resistors at 4 K connected to optically isolated battery-powered voltage sources that have a total noise of approximately 10 ppm. The resistor R_V limits the switching to a subgap voltage ~ 1 mV to minimize the generation of quasiparticles.

The initial test of this circuit measures the device parameters and finds optimum biasing. Figure 2 shows the values of I_V and I_ϕ at which the circuit switches into the voltage state. Here the bias currents follow a triangular trajectory, and the full range of currents is sampled by sweeping in time the initial ratio of I_V and I_ϕ . Analysis of the circuit shows that the center of the vertical step corresponds to the optimal bias condition $I_V = (M/L)I_\phi$ discussed previously. At this point, $I_0 = I_V$ and the ratio of the two currents is L/M . The step height is $2i_0$ and its slope is $-L/L_{Jf}$. Multiple vertical lines at the step arise

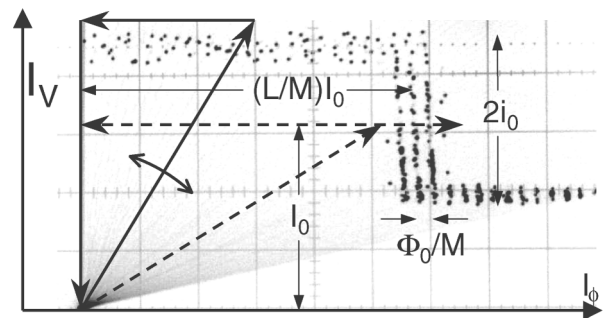


FIG. 2. Measurement of circuit parameters obtained from a plot of the I_V and I_ϕ values at which the circuit switches to the voltage state. Solid arrows indicate trajectory of the swept triangular bias for measurement mode. Dashed arrows indicate optimal biasing for normal operation.

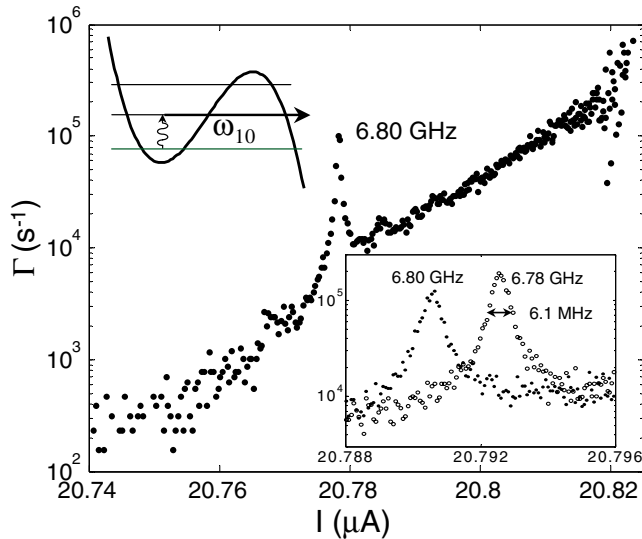


FIG. 3. Measured escape rate Γ vs junction bias current I with 6.80 GHz microwave irradiation. Lower inset shows detail of resonance for an additional frequency 6.78 GHz. Widths of resonances correspond to 6.1 MHz, giving $Q \approx 1000$. Upper inset illustrates the procedure for this spectroscopy measurement.

from flux quantization in the superconducting loop [17], with the line spacing in I_ϕ giving M .

We first determine the energy-level spacings and Q spectroscopically [2]. Figure 3 shows the measured escape rate as a function of the qubit bias current I in the presence of a microwave signal at a fixed frequency $\omega/2\pi = 6.80$ GHz. A resonance is observed because ω_{10} varies with current bias. The temperature $T \approx 25$ mK is low enough so that without microwaves the measured escape rate is consistent with the quantum-tunneling prediction Γ_0 . The resonance in the escape rate arises from the resonant increase in population of state $|1\rangle$, which tunnels at a higher rate than the ground state. Figure 3 also shows an expanded current scale for resonance curves obtained with slightly different values of $\omega/2\pi$. The full width at half maximum of these resonances is 6.1 MHz, implying a quality factor $Q \approx 1000$.

Figures 4–6 demonstrate preparation and measurement of the qubit state. For these data, $Q \approx 350$ and a bias current is selected such that $\Gamma \approx 1.2 \times 10^3$ s $^{-1}$ ($\Delta U/\hbar\omega_p \approx 2.8$) for no microwaves. The qubit remains on resonance during the entire microwave pulse sequence by using a current bias with a slow ramp rate.

The fidelity of the state measurement is determined with the data of Fig. 4. State $|1\rangle$ is populated incoherently via an excitation pulse with frequency ω_{10} , power P_{10} , and duration $0.7 \mu\text{s}$ that is much longer than the coherence time. The state measurement pulse of duration 25 ns is applied about 40 ns before the end of the excitation pulse to ensure the population does not decay before measurement. We measure the probability p_v as the ratio of the number of events that switch to the voltage state

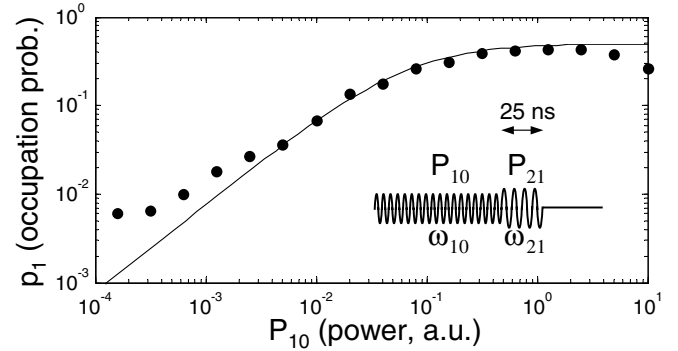


FIG. 4. Occupation probability p_1 vs microwave power P_{10} at frequency $\omega_{10}/2\pi = 6.9$ GHz, obtained for a measurement pulse of frequency $\omega_{21}/2\pi = 6.28$ GHz, power $P_{21} = 5$, and duration 25 ns. Power $P_{10}, P_{21} = 1$ (a.u.) corresponds to ~ 1 pW at $R_{\mu w}$. Theory plotted as a solid curve. Data at low power indicate fidelity of $|0\rangle$ state preparation and measurement better than 99%; saturation near 50% gives fidelity of 85% for measurement of the $|1\rangle$ state.

during the measurement pulse to the total number of events. For $P_{10} = 0$, we obtain $p_1 = 0.003$. Figure 4 shows a linear increase in the population of state $|1\rangle$ with increasing P_{10} until saturation occurs at $p_1 = 0.43 \pm 0.05$ for high power. We see good agreement between the data and the expected theoretical behavior $p_1 = 0.5/(1 + P_{\text{sat}}/P_{10})$, where the saturation power $P_{\text{sat}} = 0.065$ is chosen for best fit. We think the slight decrease in p_1 at the highest power is due to off resonant $1 \rightarrow 2$ transitions. The optimum setting of P_{21} is chosen by maximizing the ratio of p_v between $P_{10} \approx 10P_{\text{sat}}$ and $P_{10} = 0$. These results imply that the $|0\rangle$ state is prepared and measured with greater than 99% fidelity, whereas the $|1\rangle$ state is measured with 85% fidelity.

The measured relaxation rate of state $|1\rangle$ is shown in Fig. 5. Here p_1 is obtained as in Fig. 4, but with a time delay between excitation and measurement. We observe nonexponential decay, initially with rate $\sim (20 \text{ ns})^{-1}$ but later becoming significantly slower $\sim (300 \text{ ns})^{-1}$.

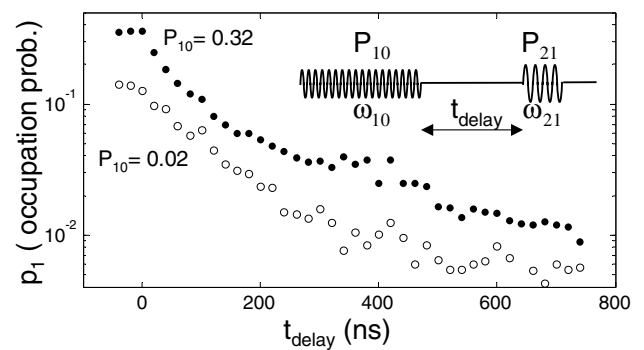


FIG. 5. Occupation probability p_1 of state $|1\rangle$ vs time delay t_{delay} between excitation and measurement pulses. Two values of initial-state population are obtained by varying the power P_{10} of the excitation pulse.

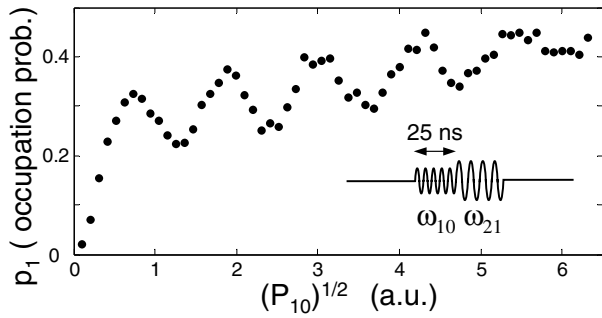


FIG. 6. Observation of Rabi oscillations from an excitation pulse of 25 ns and frequency ω_{10} followed by a measurement pulse at frequency ω_{21} . Plot shows periodic modulation of p_1 vs microwave *amplitude*, as expected from theory. The amplitude of the oscillations are maximized by using an overlap of 7 ns between the pulses.

Coherent manipulation of the qubit state is demonstrated by the observation of Rabi oscillations [7], as shown in Fig. 6. These data are obtained as in Fig. 4, but with a 25 ns excitation pulse that allows coherence to be maintained during the pulse. The phase of the Rabi oscillations is the product of the microwave amplitude and pulse length. Because the coherence time is short, the data of Fig. 6 are obtained by fixing the duration of the pulse and varying the amplitude. For an initial pulse of 17 ns (data not shown), the Rabi oscillations have similar magnitude but a period 1.36 times longer, consistent within experimental uncertainties to the ratio of the pulse widths. Full modulation of the oscillations between 0 and 1 is expected without decoherence; the observed amplitude of 15% points to a coherence time of ~ 10 ns, consistent with our other observations.

The data in Figs. 4–6 consistently give a qubit coherence time much shorter than the predicted value $4 \mu\text{s}$. Clearly, a source of noise and dissipation other than that of the circuit admittance must be present. The nonexponential energy decay possibly indicates that the qubit couples to a *small* number of other degrees of freedom that can transfer energy back to the qubit. We also observe that the measured Q randomly changes over time by a factor of ~ 2 when the junction is at base temperature 25 mK, and by a factor of ~ 4 when heated briefly to 300 mK. These observations suggest that the extra decoherence comes from dissipation in the thin (~ 2 nm) capacitor formed by the tunnel junction, probably from trap states in niobium oxides. Since long coherence and energy relaxation times have been measured in Al/Al₂O₃/Al [13] and NbN/AlN/NbN [18] tunnel junctions, we expect our qubit circuit will attain coherence times $> 1 \mu\text{s}$ after improving or changing our junction fabrication process.

In conclusion, we have devised a new Josephson-junction circuit based on large-area junctions that is a good candidate for a scalable solid-state quantum computer. This circuit uses broadband impedance transform-

ers to isolate the qubit from dissipation of the bias and measurement leads. Although decoherence is stronger than expected, proper operation has been clearly demonstrated. Observation of Rabi oscillations shows coherent manipulation of the qubit states, and preparation and measurement is accomplished with high fidelity.

We thank D. Wineland, D. Esteve, and M. Devoret for helpful discussions, and N. Bergren for fabrication of the qubit chips. This work is supported in part by NSA under Contract No. MOD709001.

*Electronic address: martinis@boulder.nist.gov

†Electronic address: urbina@cea.fr

- [1] A. J. Leggett, *Chance and Matter*, edited by J. Souletie, J. Vannimenus, and R. Stora (Elsevier, Amsterdam, 1987), p. 395.
- [2] J. M. Martinis, M. H. Devoret, and J. Clarke, *Phys. Rev. Lett.* **55**, 1543 (1985).
- [3] J. Clarke, A. N. Cleland, M. H. Devoret, D. Esteve, and J. M. Martinis, *Science* **239**, 992 (1988).
- [4] V. Bouchiat, D. Vion, P. Joyez, D. Esteve, and M. H. Devoret, *Phys. Scr.* **T76**, 165 (1998).
- [5] Y. Nakamura, C. D. Chen, and J. S. Tsai, *Phys. Rev. Lett.* **79**, 2328 (1997).
- [6] J. R. Friedman, V. Patel, W. Chen, S. K. Tolpygo, and J. E. Lukens, *Nature (London)* **406**, 43 (2000).
- [7] M. A. Nielsen and I. L. Chuang, *Quantum Computation and Quantum Information* (Cambridge University Press, Cambridge, 2000).
- [8] Y. Makhlin, G. Schön, and A. Shnirman, *Rev. Mod. Phys.* **73**, 357 (2001).
- [9] J. E. Mooij, T. P. Orlando, L. Levitov, L. Tian, C. H. van der Wal, and S. Lloyd, *Science* **285**, 1036 (1999).
- [10] F. C. Wellstood, C. Urbina, and J. Clarke, *Appl. Phys. Lett.* **50**, 772 (1987).
- [11] G. Zimmerli, T. M. Eiles, R. L. Kautz, and J. M. Martinis, *Appl. Phys. Lett.* **61**, 237 (1992); A. B. Zorin, F. J. Ahlers, J. Niemeyer, T. Weimann, H. Wolf, V. A. Krupenin, and S. V. Lotkhov, *Phys. Rev. B* **53**, 13 682 (1996).
- [12] Y. Nakamura, Y. A. Pashkin, T. Yamamoto, and J. S. Tsai, *Phys. Rev. Lett.* **88**, 047901 (2002).
- [13] D. Vion, A. Aassime, A. Cottet, P. Joyez, H. Pothier, C. Urbina, D. Esteve, and M. H. Devoret, *Science* **296**, 886 (2002).
- [14] D. Esteve, M. H. Devoret, and J. M. Martinis, *Phys. Rev. B* **34**, 158 (1986).
- [15] When the qubit junction switches to the voltage state, the loop current I is interrupted. Because $I_V > i_0$, the filter junction then also switches.
- [16] J. M. Martinis, M. H. Devoret, and J. Clarke, *Phys. Rev. B* **35**, 4682 (1987).
- [17] Although here we analyze data from one value of the quantized flux, annealing techniques can reset the flux to only one value. See V. Lefevre-Seguin, E. Turlot, C. Urbina, D. Esteve, and M. H. Devoret, *Phys. Rev. B* **46**, 5507 (1992).
- [18] S. Han, Y. Yu, Xi Chu, S. Chu, and Z. Wang, *Science* **293**, 1457 (2001); Y. Yu, S. Han, X. Chu, S. Chu, and Z. Wang, *Science* **296**, 889 (2002).